Available online at www.sciencedirect.com
SCIENCE DIRECT®
Journal of Contaminant Hydrology 65 (2003) 161–182
JOURNAL OF Contaminant Hydrology
www.elsevier.com/locate/jconhyd

# Colloid transport in a geochemically heterogeneous porous medium: aquifer tank experiment and modeling

Jonathan P. Loveland[a], Subir Bhattacharjee[b], Joseph N. Ryan[a,*], Menachem Elimelech[c]

[a] *Department of Civil, Environmental, and Architectural Engineering, University of Colorado, Campus Box 428, Boulder, CO 80309-0428, USA*
[b] *Department of Mechanical Engineering, University of Alberta, Edmonton, Alberta, Canada, T6G 2G8*
[c] *Department of Chemical Engineering, Environmental Engineering Program, P.O. Box 208286, Yale University, New Haven, CT 06520-8286, USA*

Received 27 November 2001; received in revised form 6 November 2002; accepted 13 November 2002

**Abstract**

To examine colloid transport in geochemically heterogeneous porous media at a scale comparable to field experiments, we monitored the migration of silica-coated zirconia colloids in a two-dimensional layered porous media containing sand coated to three different extents by ferric oxyhydroxides. Transport of the colloids was measured over 1.65 m and 95 days. Colloid transport was modeled by an advection–dispersion–deposition equation incorporating geochemical heterogeneity and colloid deposition dynamics (blocking). Geochemical heterogeneity was represented as favorable (ferric oxyhydroxide-coated) and unfavorable (uncoated sand) deposition surface areas. Blocking was modeled as random sequential adsorption (RSA). Release of deposited colloids was negligible. The time to colloid breakthrough after the onset of blocking increased with increasing ferric oxyhydroxide-coated surface area. As the ferric oxyhydroxide surface area increased, the concentration of colloids in the breakthrough decreased. Model-fits to the experimental data were made by inverse solutions to determine the fraction of surface area favorable for deposition and the deposition rate coefficients for the favorable (ferric oxyhydroxide-coated) and unfavorable sites. The favorable deposition rate coefficient was also calculated by colloid filtration theory. The model described the time to colloid breakthrough and the blocking effect reasonably well and estimated the favorable surface area fraction very well for the two layers with more than 1% ferric oxyhydroxide coating. If mica edges in the uncoated sand were considered as favorable surface area in addition to the ferric oxyhydroxide coatings, the model

* Corresponding author. Tel.: +1-303-492-0772; fax: +1-801-327-7112.
*E-mail address:* joseph.ryan@colorado.edu (J.N. Ryan).

0169-7722/02/$ - see front matter © 2002 Elsevier Science B.V. All rights reserved.
doi:10.1016/S0169-7722(02)00238-3

predicted the favorable surface area fraction accurately for the layer with less than 1% ferric oxyhydroxide coating.
© 2002 Elsevier Science B.V. All rights reserved.

*Keywords:* Colloid; Transport; Modeling; Ferric oxyhydroxide; Geochemical heterogeneity

## 1. Introduction

The transport of colloids, pathogenic microbes, and colloid-associated contaminants has spurred the development of models of colloid transport in subsurface environments. Initially, these models portrayed the attachment of colloids (and "biocolloids") to aquifer grain surfaces as equilibrium sorption (Yates et al., 1987; Mills et al., 1991). Later, colloid filtration (irreversible first-order attachment) was introduced in conjunction with equilibrium sorption in two-site models (Harvey and Garabedian, 1991; Bales et al., 1991). In most cases, colloid transport in homogeneous porous media was adequately characterized by first-order attachment and release (Hornberger et al., 1992; Corapcioglu and Jiang, 1993). Further advances have focused on three factors affecting colloid deposition kinetics: (1) the dynamics of particle deposition (blocking and ripening), (2) the geochemical heterogeneity of aquifer grain surfaces, and (3) the physical heterogeneity of the porous medium (Ryan and Elimelech, 1996). The blocking effect was included in colloid transport models as linear Langmuirian attachment (Privman et al., 1991; Song and Elimelech, 1993; Saiers et al., 1994a) and nonlinear random sequential adsorption (Johnson and Elimelech, 1995). The geochemical heterogeneity effect was included as random or patchwise distributions of different surface charge (Song and Elimelech, 1994; Johnson et al., 1996). The physical heterogeneity effect was included as structured and random distributions of hydraulic conductivity (Saiers et al., 1994b; Rehmann et al., 1999; Sun et al., 2001a) fractures (Grindrod, 1993; Abdel-Salam and Chrysikopoulos, 1995), and the correlation of colloid transport parameters with hydraulic conductivity (Ren et al., 2000; Sun et al., 2001a).

Experimental studies of the effects of geochemical and physical heterogeneity and deposition dynamics on colloid transport have been conducted primarily in laboratory columns of less than 10 cm length. Several field tests of colloid and "biocolloid" transport have been conducted (e.g., Harvey and Garabedian, 1991; Higgo et al., 1993; Schijven and Hassanizadeh, 2000), but most of these did not directly investigate either heterogeneity, because adequate aquifer sediment characterization was lacking, or deposition dynamics, because injections of colloids were made as relatively short-term pulses. Ryan et al. (1999) showed that geochemical heterogeneity in the form of ferric oxyhydroxide-coated sands controlled the transport of silica colloids and the virus, but transport was tracked only over a 1-m distance. Schijven et al. (2000) determined that spatially varying distributions of ferric oxyhydroxides limited the transport of microbes in a bank filtration setting.

To better investigate heterogeneity and deposition dynamics at a scale representative of natural conditions, we conducted colloid transport experiments in a geochemically heterogeneous porous medium comprised of layers of ferric oxyhydroxide-coated sand

assembled in a two-dimensional aquifer tank (a slice of an aquifer). In the aquifer tank, geochemical and physical heterogeneities can be created, and colloid transport experiments can be readily replicated. Silica-coated zirconia colloids were employed as a readily traced model of negatively charged natural colloids. We modeled the results with a recently developed two-dimensional colloid transport model that incorporates heterogeneity and deposition dynamics (Sun et al., 2001a,b).

## 2. Materials and methods

A continuous step injection of silica-coated zirconia colloids was made into a geochemically heterogeneous porous medium contained in a two-dimensional aquifer tank. The porous medium consisted of three layers of sand coated by different amounts of iron oxyhydroxides. The transport of the colloids was measured over 95 days in 144 sampling ports.

### 2.1. Silica-coated zirconia colloids

Silica-coated zirconia ($ZrO_2$) colloids were used in this experiment for ease and sensitivity of detection (Ryan et al., 2000). Spherical zirconia colloids (20% $ZrO_2$ colloidal dispersion, pH 3 nitric acid solution, Alfa ÆSAR) of about 110 nm in diameter were coated with silica by hydrolysis of tetramethyl orthosilicate (99+%, Aldrich) in an ethanol/ammonium hydroxide solution. A stock suspension of the silica-coated colloids was created by resuspending the colloids in a $10^{-3}$ M NaCl solution (pH $\sim$ 5.7) prepared with high-purity water (Millipore Milli-Q). The stock suspension was refrigerated at 4 °C until use.

The size and zeta potential of the influent colloid suspension were measured at the beginning and during the experiment. The mean and standard deviation of the colloid diameter was $150 \pm 30$ nm as determined by dynamic light scattering (Particle Sizing Systems, Nicomp 370). Most of the standard deviations represent polydispersity in the colloid size. The zeta potential of the colloids ($-33 \pm 3$ mV) was measured by laser Doppler microelectrophoresis (Brookhaven, Zeta-Plus). No significant changes in colloid size or zeta potential were detected in the influent colloid suspension during the experiment.

### 2.2. Ferric oxyhydroxide-coated sand

The porous medium was composed of mixtures of uncoated and ferric oxyhydroxide-coated sand. The subangular to angular uncoated sand (Unimin, 4060 sand) has a mean diameter ($d_{50}$) of 0.50 mm, a $d_{10}$ value of 0.37 mm, and a uniformity coefficient ($d_{60}/d_{10}$) of 1.4. The mineralogical composition, as determined by petrographic microscopy of a thin section of the sand, is predominantly quartz (80%), feldspars (11%), muscovite/biotite (8%), and trace heavy minerals (1%).

The coated sand was prepared by precipitating ferric oxyhydroxides on the sand surface. Batches of the sand (20 kg) were suspended in 20 l of 0.1 M ferric nitrate solution in an acid-cleaned concrete mixer. While the mixer was rotating at about 30 rpm, the

suspension was titrated with 0.1 M sodium hydroxide solution at a rate of 1 l $h^{-1}$ until the pH reached 7.0. After another hour of mixing, excess solution was decanted and the coated sand was heated at 105 °C until dry. X-ray diffraction (Scintag, model XPH-105; Cu $K_\alpha$ radiation, 2°2$\theta$ $min^{-1}$, 0–60°2$\theta$) on a crushed sample of the coated sand revealed goethite (α-FeOOH) as the only iron-containing mineral.

Thin sections (30 μm × 3 × 3 cm) of coated sand grains were prepared by setting the grains in epoxy resin. Electron microprobe/backscatter electron imaging (JEOL, JXA-8600, 15 kV accelerating voltage) and energy-dispersive X-ray analysis of carbon-coated thin sections revealed thin (1–10 μm) iron-rich rinds coating an average of 75 ± 5% of the surface of virtually all of the grains (Fig. 1). These coatings did not significantly change the average size or shape of the sand grains.

To create a geochemically heterogeneous porous medium in the aquifer tank, dry portions of uncoated and coated sand were tumbled in the concrete mixer in proportions of 0.1, 5.0, and 10.0 wt.% coated sand for 2 h. The range of mixture proportions (Table 1) was designed to bracket the 3–4% coverage of ferric oxyhydroxide coating found on sand grains from the Cape Cod, MA, aquifer in which we have conducted colloid and virus transport experiments (Pieper et al., 1997; Ryan et al., 1999). Fractional surface coverage by the ferric oxyhydroxide coating was measured by electron microprobe/backscatter electron detection. With backscatter electron detection, the ferric oxyhydroxide coatings appeared as bright rims on dark gray grains (Fig. 1). The 3 × 3 cm thin section was divided into 36 sections of 5 × 5 mm. In each section, the total and coated grains were counted, and the fractional surface coverage of the coated grains was estimated. Grains smaller than 63 μm and heavy mineral grains were not counted. A minimum of 4000 grains was counted for each thin section. In addition, the reducible ferric oxyhydroxide fraction was measured in triplicate samples for the coated and uncoated sand and each mixed layer by Ti(III)–citrate–EDTA extraction (Ryan and Gschwend, 1991).

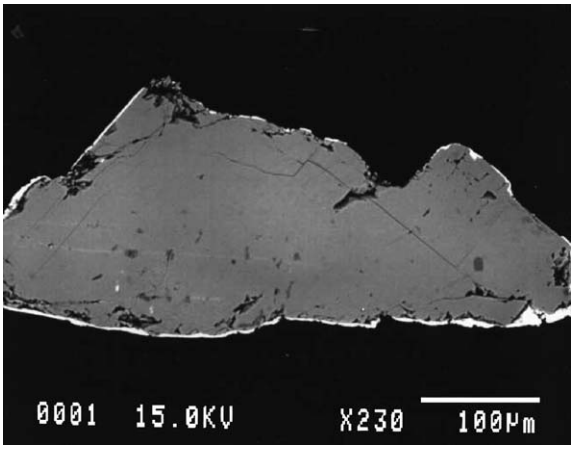


Fig. 1. Electron microprobe/backscatter electron image of a quartz grain synthetically coated by ferric oxyhydroxide (magnification, 230 times; 100 μm scale bar). Energy-dispersive X-ray analysis confirmed that the bright rind revealed by backscatter electron imaging contains primarily iron, and that the dark grain contains primarily silicon.

Table 1
Mixing proportions, reducible Fe(III) content, and estimated, measured, and model-fit values of the favorable surface area fraction $\lambda$ for the three layers of sand and the coated and uncoated sands used in the aquifer tank

| Layer/grain | Coated sand/total sand (wt.%) | Fe(III) content[a] (mmol $kg^{-1}$) | Estimated[b] favorable surface area fraction $\lambda$ (%) | Measured[c] favorable surface area fraction $\lambda$ (%) | Model-fit[d] favorable surface area fraction | |
|---|---|---|---|---|---|---|
| | | | | | Method 1 $\lambda$ (%) | Method 2 $\lambda$ (%) |
| Upper layer | 0.1 | $2.9 \pm 0.6$ | 0.075 | 0.14 | $1.2 \pm 0.8$ | $1.7 \pm 0.7$ |
| Middle layer | 10 | $6.6 \pm 2.5$ | 7.5 | 8.3 | $9.1 \pm 0.5$ | $9.2 \pm 1.0$ |
| Lower layer | 5.0 | $4.6 \pm 1.0$ | 3.8 | 4.2 | $3.8 \pm 0.9$ | $4.0 \pm 0.8$ |
| Coated grains | 100 | $19.5 \pm 1.5$ | – | $75 \pm 5$ | – | – |
| Uncoated grains | 0 | $3.6 \pm 0.6$ | – | 0 | – | – |

[a] Measured by Ti(III)–citrate–EDTA extraction of reducible ferric oxyhydroxides.
[b] Estimated as the product of the coated sand/total sand ratio and an average of 75% ferric oxyhydroxide coating on each coated grain.
[c] Measured by electron microprobe analysis of thin sections, 4000–4820 total grains.
[d] Estimated by optimal model fit to colloid breakthrough curves, where method 1 was fit by a complete inverse solution of $k_f$, $k_u$, $\lambda_{upper}$, $\lambda_{middle}$, and $\lambda_{lower}$, and method 2 was fit by calculating $k_f$ according to colloid filtration theory and inverse solution of $k_u$, $\lambda_{upper}$, $\lambda_{middle}$, and $\lambda_{lower}$.

### 2.3. Aquifer tank setup

The colloid transport experiments were conducted in an acrylic (0.30 cm thick) tank of 5.0 m length, 1.0 m height, and 0.10 m width (Fig. 2). Lateral members buttress the tank to prevent wall deflection. At each end of the tank, flow control reservoirs (0.25 m length) were separated from the porous medium by nylon mesh laminated in a polyethylene frame. In the influent reservoir, a fixed overflow outlet controlled water level. In the effluent reservoir, water level was controlled by a constant head reservoir connected to the tank outlet by Tygon® tubing. The influent colloid suspension was prepared in the mixing barrel (200 l polyethylene) and pumped into the influent barrel at the beginning of the experiment and during each refill. The contents of the influent barrel were constantly circulated through the influent reservoir at a flow rate of 8 l $h^{-1}$.

Samples of pore water were obtained through stainless steel hypodermic needles (16 gauge, 10 cm length) fitted to the tank with a compression fitting, ferrules, and polycarbonate three-way stopcock. The needle tips were inserted 5 cm into the 10-cm-wide porous medium. Some sampling ports were also fitted with piezometers (vertical Tygon® tubes attached to the stopcocks) to check the uniformity of the hydraulic gradient over the length of the tank.

### 2.4. Aquifer tank packing

The tank was filled with three layers of partially coated sand mixtures using a wet packing technique. Deionized water was pumped into the tank to a height of 10 cm, and a layer of 5.0 wt.% ferric oxyhydroxide-coated sand was poured into the water to a height of 5 cm. The layer was gently consolidated with a $10 \times 10$ cm acrylic tamper. Additional 5 cm layers of water followed by sand were placed in the tank until the 5.0 wt.% sand layer

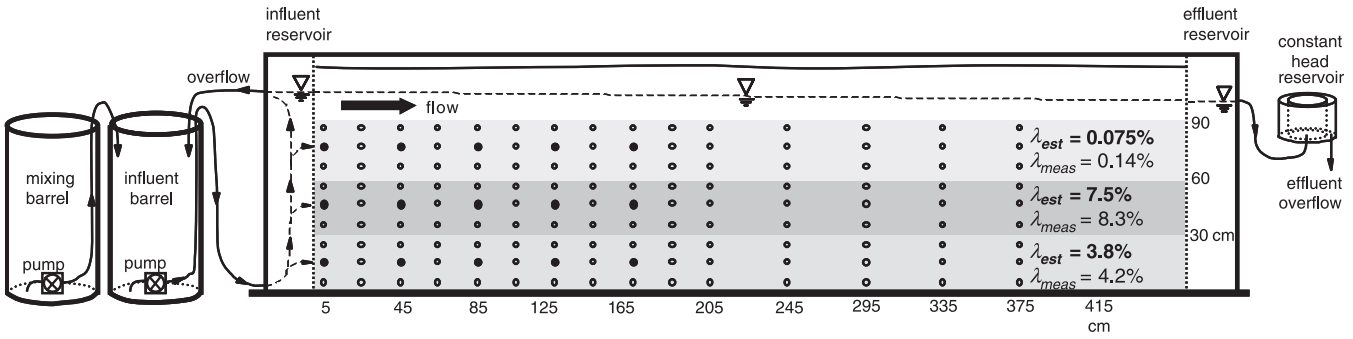


Fig. 2. Diagram of two-dimensional aquifer tank. Influent colloid suspensions were prepared in the mixing barrel and pumped into the influent barrel. Suspensions in the influent barrel were circulated through the influent reservoir. The head gradient was controlled by setting the height of the constant head reservoir. Three layers of ferric oxyhydroxide-coated sand filled the 10-cm-wide tank. Sample ports are shown as open and filled circles; data from the filled circles are shown in Fig. 3.

reached a height of 30 cm. Layers of 10.0 and 0.1 wt.% sand were placed above the 5.0 wt.% layer to heights of 30 cm each in the same manner. Finally, a 20-cm-height layer of uncoated sand was placed above the partially coated layers (transport in this layer was not monitored). After packing, the tank was flushed with a pH 11.0 NaOH solution at a high flow velocity (about 2 m $day^{-1}$) until the turbidity in the tank effluent decreased to 1 NTU (Hach, model Ratio X/R); then, a pH 5.0 solution was flushed through the tank until the effluent pH decreased to below neutral. Finally, the experimental solution ($10^{-3}$ M NaCl solution in deionized water, pH adjusted to 6.2 with NaOH) was flushed through the tank at 0.5 m $day^{-1}$ until the effluent pH and specific conductance matched those of the influent solution.

For the experiment, a constant drop in head of 0.55 cm across the length of the porous medium (447 cm) produced a flow rate of $25.0 \pm 0.3$ l $day^{-1}$. With an average cross-sectional area of the porous medium of 1020 $cm^2$, the hydraulic conductivity was $200 \pm 2$ m $day^{-1}$. A porosity of 0.459 was measured by determining the volume of water displaced by sand after duplicating the packing method in a 20-l bucket. The resulting pore velocity was $0.53 \pm 0.01$ m $day^{-1}$.

### 2.5. Colloid transport experiment

The influent colloid suspension was prepared in the mixing barrel by adding the colloid suspension and tritiated water ($^3$HHO, DuPont NeN, 1.0 mCi $ml^{-1}$ specific activity, diluted to 10.0 μCi $ml^{-1}$ for additions) to the experimental solution ($10^{-3}$ M NaCl, pH 6.2). The initial colloid concentration in the influent suspension was 23.2 mg Zr $l^{-1}$. The estimated total mass concentration of the colloids is 52 mg $l^{-1}$ (using particle Zr concentration, size, $SiO_2/ZrO_2$ ratio, and density; Ryan et al., 2000). The tritium activity in the influent suspension was 320 pCi $ml^{-1}$ (710 disintegrations $min^{-1}$ $ml^{-1}$). The suspension was mixed by rapid recirculation of the suspension with a submersible pump until uniform turbidity (Hach, Ratio X/R) and pH were achieved in the mixing barrel. After mixing, the colloid suspension was pumped into the influent barrel and recirculated into the influent flow control reservoir. Time zero was marked for the experiment when the turbidity in the influent flow control reservoir matched the turbidity in the influent barrel. Filling the influent reservoir with the injection suspension required 16 min.

Samples were collected twice daily from sampling ports in the center of the three layers (upper, middle, and lower) at transport distances of 5, 45, 85, 125, and 165 cm (Fig. 2) and during times when tracer and colloid breakthroughs were expected. The expected breakthrough times were predicted by the colloid transport model with parameters estimated from preliminary column experiments. Samples were also collected every other day from ports near the layer boundaries at times when breakthroughs were expected. A volume of 20 ml of pore water was collected for each sample by opening the stopcock and allowing water to drain into a polyethylene bottle.

### 2.6. Sample analyses

Each sample was analyzed for colloid concentration and tritium activity. Colloid concentration was measured in 10 ml portions of each sample acidified with concentrated nitric acid (1 ml), stored for at least 1 day, and analyzed for zirconium by inductively

coupled plasma–atomic emission spectroscopy (Varian, Liberty Series II AX-150; detection limit, 1.5 μg $l^{-1}$). Tritium concentration was measured by adding scintillation cocktail (10 ml, Packard Gold XR) to 10 ml portions of each sample and analyzing tritium activity by liquid scintillation counting (Packard, model Tri-Carb 2300TR). The size and zeta potential of the colloids and the pH and specific conductance of the pore waters were tested daily in the influent and effluent reservoirs and in selected samples. Less frequent sampling was also done for total iron concentration (measured by ICP-AES) and turbidity in the effluent reservoir.

## 3. Modeling and parameter estimation

In this section, we outline the mathematical model emulating the colloid transport experiments and the method for identification of the colloid deposition parameters in the geochemically heterogeneous porous medium used in the experiments. The modeling approach and the inverse problem of parameter identification have been described in considerable detail elsewhere (Sun et al., 2001a,b). This section delineates some of the key features of the model and modifications in the parameter estimation technique pertinent to the present work.

### *3.1. Model formulation and boundary conditions*

Colloid transport in a porous medium is modeled as a combination of three mechanisms: (1) advection, (2) dispersion, and (3) attachment to the collector surfaces. In a geochemically heterogeneous porous medium, the total available collector surface area for colloid deposition will be composed of different types of surface area (or patches) that exhibit different affinities for the colloids. For this experiment, we assume that surface area of the collectors was comprised of two fractions: ferric oxyhydroxide coatings and the uncoated surfaces of the sand. The two surfaces exhibit very different affinity for the colloids owing to electrostatic attraction and repulsion. Under the experimental conditions (pH 6.2), the silica-coated zirconia colloid surfaces are negatively charged, the ferric oxyhydroxide surfaces are positively charged, and the sand (mainly quartz, feldspars, and mica) surfaces are negatively charged; hence, colloids are electrostatically attracted to the ferric oxyhydroxide coatings (the favorable surface area fraction $\lambda$) and repelled from the uncoated sand surfaces (the unfavorable surface area fraction, $1-\lambda$).

The generalized colloid transport equation accounting for patchwise geochemical heterogeneity is (Johnson et al., 1996; Sun et al., 2001a):

$$\frac{\partial n}{\partial t} = \nabla \cdot (\mathbf{D} \cdot \nabla n) - \nabla \cdot (\mathbf{V} n) - \frac{f}{\pi a_p^2}\left[\lambda \frac{\partial \theta_f}{\partial t} + (1-\lambda)\frac{\partial \theta_u}{\partial t}\right] \quad (1)$$

where $n$ is the number concentration of the colloids in suspension, $\mathbf{D}$ is the dispersion tensor, $\mathbf{V}$ is the interstitial fluid velocity vector, $f$ is the specific surface area of the collector grains, $a_p$ is the colloid particle radius, $\lambda$ is the fraction of total surface area on which attachment is favorable (the "heterogeneity parameter"), and $\theta$ is the fractional surface

coverage of colloids on the collector surfaces for the favorable ($\theta_f$) and unfavorable ($\theta_u$) regions.

The initial and boundary conditions for the colloid transport equation were specified as (1) the porous medium colloid concentrations were initially set to zero ($n=0$, $\theta_f=\theta_u=0$), (2) zero dispersive flux boundary conditions were specified at the domain boundaries, and (3) a given concentration of colloids was line-injected at the up-gradient vertical boundary at $t>0$ (Sun et al., 2001a). Following the procedure of colloid injection in the experiments, a continuous line injection was set as a fixed concentration boundary condition at the inlet of the rectangular domain for the two-dimensional model.

### 3.2. Blocking and release

The surface coverage rates in Eq. (1) are related to the rates of colloid deposition by kinetic expressions of the form (Johnson et al., 1996)

$$\frac{\partial \theta_f}{\partial t} = \pi a_p^2 k_f n B(\theta_f) \tag{2a}$$

$$\frac{\partial \theta_u}{\partial t} = \pi a_p^2 k_u n B(\theta_u) \tag{2b}$$

where $k_f$ and $k_u$ are the deposition rate constants on the favorable and unfavorable surfaces, respectively. The term $B(\theta)$ is a dynamic blocking function that relates the transient reduction in colloid deposition rates to the reduced availability of sites for deposition. Employing the random sequential adsorption (RSA) model, the blocking function was expressed as a virial expansion in the fractional surface coverage

$$B(\theta) = 1 + a_1\theta + a_2\theta^2 + a_3\theta^3 + \cdots \tag{3}$$

where $a_1$, $a_2$, and $a_3$ are $-4$, $6\sqrt{3}/\pi$, and 1.404, respectively (Johnson et al., 1996; Ko et al., 2000). For the background electrolyte concentration (1 mM) and flow velocity (about 0.5 m day$^{-1}$) used in this experiment, we do not expect a significant deviation of the RSA virial coefficients from these "hard-sphere" values.

Release of colloids from the porous media was also considered for colloids deposited on the unfavorable quartz grain surfaces. Deposition of the negatively charged silica-coated colloids to the ferric oxyhydroxide patches was considered to be irreversible (Loveland et al., 1996). To portray release of colloids from the quartz surfaces, the following term was incorporated as a modification of Eq. (2b):

$$\frac{\partial \theta_u}{\partial t} = \pi a_p^2 k_u n B(\theta_u) - k_r \theta_u \tag{4}$$

where $k_r$ is the first-order release rate coefficient.

### 3.3. Numerical procedures

The colloid advection–dispersion–deposition equation (Eq.(1)) was solved in both one- and two-dimensional forms. Because this experiment resulted in predominantly one-

dimensional (horizontal) flow with negligible transverse dispersion, the one-dimensional form of the equation was used for parameter identification in each layer. The two-dimensional form was used to study the extent by which inclusion of transverse dispersion could affect the estimated transport and deposition parameters.

The governing one-dimensional colloid transport equation was solved using the method of lines (Zwillinger, 1989). The one-dimensional advection–dispersion equation was discretized in the spatial domain using the finite difference method. This yields a series of coupled ordinary differential equations (ODEs) in time at each spatial node, which can be solved simultaneously employing a backward difference scheme (Petzold, 1982; Bhattacharjee et al., 1999). It should be noted that the sink term (in square brackets) in Eq. (1) is a combination of two additional differential equations (Eqs. (2a), (2b), and (3)) relating colloid deposition on favorable and unfavorable surfaces to colloid removal from the dispersed phase. Hence, at each spatial location, we solved three coupled ODEs, one stemming from the discretized advection–dispersion equation and two stemming from the deposition rate equations.

The two-dimensional form of Eq. (1) was solved for a steady horizontal flow field using an upstream weighted multiple cell balance technique (Sun et al., 2001a). The rectangular domain was discretized using linear triangular elements. The finite element mesh was designed to match element boundaries with the layer boundaries. Because there was no physical heterogeneity in the experiments, the flow was computed using a fixed set of hydrologic parameters for the entire domain. The set of ordinary differential equations in time derived from the spatially discretized equations were solved using a Crank–Nicholson technique.

A modified Levenberg–Marquardt technique (More et al., 1980) was used to minimize the sum-square errors between the experimental and predicted values of the colloid concentration at different observation wells in the tank. The one-dimensional model for colloid transport and deposition was used to solve the forward problem. The parameter phase space was constrained such that the deposition rate constants were never allowed to become negative. The heterogeneity parameter was limited by $0 < \lambda < 50\%$ to prevent ambiguity in the model arising from the correlation between the deposition rate constants and the heterogeneity parameter.

### 3.4. Estimation of hydrologic parameters

The longitudinal dispersivity $\alpha_L$ was determined by fitting the breakthrough of tritiated water in six breakthrough curves (45 and 85 cm transport distances in the three layers) using a one-dimensional form of the advection–dispersion equation (Eq. (1) without deposition). Breakthroughs from the 45- and 85-cm transport distances were used exclusively because tracer breakthrough measurements at the other transport distances were less complete (Fig. 3). For these fits, hydraulic conductivity was set at 200 m $day^{-1}$ as estimated by Darcy's Law with experimental data. From the six values of $\alpha_L$ determined by one-dimensional fits of the breakthrough curves, a single mean value of $\alpha_L$ was calculated (Table 2). Simulated breakthrough curves produced using this mean value of $\alpha_L$ in both one-dimensional and two-dimensional transport models closed agreed with the breakthrough curves measured at all transport distances. The effect of the transverse dispersivity $\alpha_T$ on tracer transport was

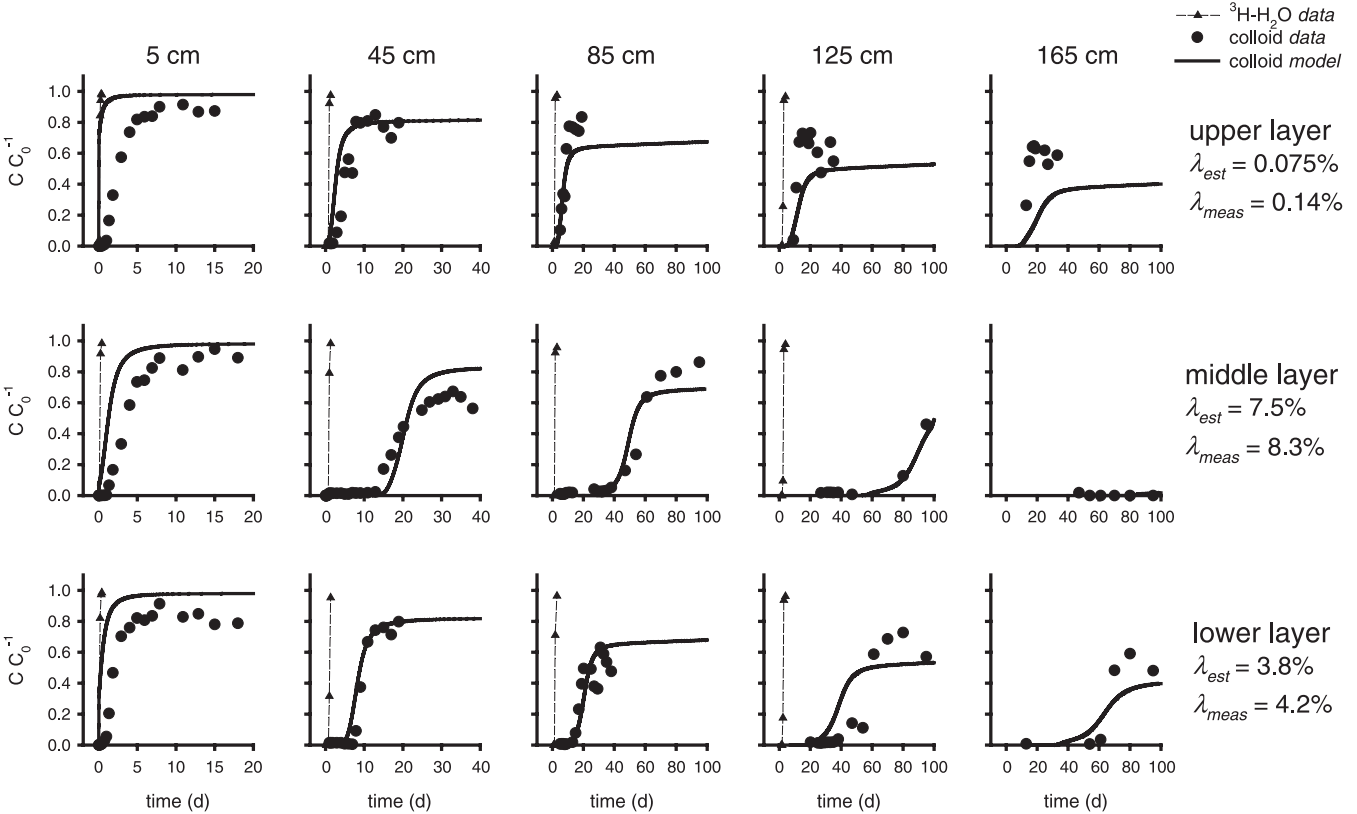


Fig. 3. Tracer and colloid concentrations normalized by the influent concentration ($C\ C_0^{-1}$) as a function of time. Best fits produced by the colloid transport model are shown as solid curves. Travel distance is listed along the top of the graphs. Favorable surface coating fraction estimates ($\lambda_{est}$) and measured values ($\lambda_{meas}$) are listed along the right side of the graphs representing each of the three layers in the aquifer tank (Fig. 2). Tracer breakthrough was not measured at the 165-cm transport distance.

Table 2
Parameters used in modeling the transport of the tritium tracer and silica-coated zirconia colloids in the aquifer tank

| Parameter | Value |
|---|---|
| Hydraulic gradient $\nabla h$ | 0.0012 |
| Hydraulic conductivity $K$ (m day$^{-1}$) | 200 |
| Porosity $\varepsilon$ | 0.46 |
| Interstitial velocity $V$ (m day$^{-1}$) | 0.53 |
| Specific storage $S_S$ | 0.0001 |
| Longitudinal dispersivity $\alpha_L$ (m) | $8.5 \times 10^{-4}$ |
| Ratio of dispersivities $\alpha_L/\alpha_T$ | 10 |
| Grain diameter $d_c$ (mm) | 0.50 |
| Specific surface area[a] $f$ (m$^2$ m$^{-3}$) | $1.4 \times 10^4$ |
| Colloid diameter $d_p$ (μm) | 0.15 |
| Colloid density (g cm$^{-3}$) | 5.1 |
| Porous medium bulk density $\rho_b$ (g cm$^{-3}$) | 1.89 |
| Influent colloid concentration $C_0$ (mg l$^{-1}$) | $23.2 \pm 1.8$ |
| Influent colloid number concentration $n_0$ (l$^{-1}$) | $2.57 \pm 0.20 \times 10^{12}$ |
| Maximum attainable surface coverage $\theta^b_{max}$ | 0.20 |

[a] Determined from $6(1-\varepsilon)/\varepsilon d_c$, where $\varepsilon$ is the porosity of the porous medium and $d_c$ is the diameter of the collector grains.
[b] Typical value based on colloid size and ionic strength (Johnson et al., 1996).

assessed in two-dimensional simulations in which $\alpha_T$ was varied from zero to $\alpha_L/10$. No perceptible change in the simulated tracer breakthrough was observed; therefore, $\alpha_T$ was set to a value of $\alpha_L/10$ (Table 2). Garabedian et al. (1991) determined that $\alpha_T$ never exceeded $\alpha_L/10$ in the Cape Cod aquifer that this aquifer tank intended to represent.

This combined one- and two-dimensional approach to the estimation of the longitudinal and transverse dispersivity was deemed appropriate given the sparseness of the tracer breakthrough data. With the data available, a full two-dimensional fitting of $\alpha_L$ and $\alpha_T$ would have resulted in very little confidence in the fitted value of $\alpha_T$.

### 3.5. Estimation of colloid transport parameters

Simultaneous estimation of the colloid transport parameters by a two-dimensional inverse analysis was attempted following the method presented by Sun et al. (2001b), but confidence levels for the estimated parameters were unacceptable. As Sun et al. (2001b) concluded, the three colloid transport parameters ($k_f$, $k_u$, $\lambda$) cannot be uniquely identified by a simultaneous inverse analysis because the three colloid transport parameters each affect the overall rate of colloid removal by deposition. Furthermore, the limited amount of breakthrough data adversely affected the two-dimensional inverse analysis. Limited breakthrough data was the result of limited sampling frequency. Sampling frequency was limited to avoid removing a significant fraction of the injected colloid mass.

The colloid transport parameters ($k_f$, $k_u$, $\lambda_{upper}$, $\lambda_{middle}$, and $\lambda_{lower}$) were determined by fitting the nine colloid breakthroughs at the 45-, 85-, and 125-cm distances using a one-dimensional form of Eq. (1). The parameter estimates were validated by two-dimensional simulations of the colloid breakthroughs. A similar approach was used by Zhang et al.

(1998) to model variable density flow and solute transport at the Cape Cod site. Colloid breakthroughs at the 5 and 165 cm distances were not used owing to possible problems with the development of uniform flow at 5 cm and incomplete colloid breakthrough data at 165 cm. First, a one-dimensional inverse analysis was performed on the nine colloid breakthroughs to estimate $k_f$, $k_u$, and $\lambda$ for each sampling port. Average $k_f$ and $k_u$ values were determined as the mean of the nine estimated values of $k_f$ and $k_u$. These average values of $k_f$ and $k_u$ were applied for each layer because each layer was composed of the same favorable and unfavorable porous media. Estimates of $\lambda$ for each sampling port were refined using the average $k_f$ and $k_u$ values in the inverse analysis with $\lambda$ as the only adjustable parameter. Finally, average values of $\lambda$ were determined for each layer ($\lambda_{upper}$, $\lambda_{middle}$, and $\lambda_{lower}$) as the mean of the three values of $\lambda$ estimated for each layer.

The deposition parameters were also estimated by assuming that the favorable deposition rate coefficient $k_f$ could be calculated independently using colloid filtration theory (Yao et al., 1971; Elimelech et al., 1995):

$$k_f = \frac{\eta_f V}{4\varepsilon} = \frac{\alpha_f \eta_0 V}{4\varepsilon} \tag{5}$$

where $\eta_f$ is the single collector efficiency for the favorable attachment surface area, $\eta_0$ is the single collector efficiency in the absence of colloidal interactions, $\alpha_f$ is the collision efficiency for the favorable attachment surface area, $V$ is the approach velocity, and $\varepsilon$ is the porosity of the porous medium (Table 2). To calculate $k_f$, we set $\alpha_f = 1$ (every collision with favorable attachment surface area resulted in attachment) and calculated $\eta_0$ for removal by the convective diffusion mechanism. Calculation of $k_f$ rendered the inverse problem considerably more facile because only $k_u$ and $\lambda$ were varied to fit each of the nine colloid breakthrough curves. The calculated value of $k_f$ and a mean value of $k_u$ (from nine values of $k_u$ determined by fitting the colloid breakthrough curves) were used to estimate values of $\lambda$ for each layer as described above.

With the release term (Eq. (4)) incorporated into the colloid transport equation, parameter estimation was done by calculating $k_f$ with colloid filtration theory and simultaneously optimizing $k_u$, $k_r$, and $\lambda$ for each experimental breakthrough curve. Release rate coefficients estimated by this method were small, indicating that release was negligible in the experiment. Incorporation of release did not yield better agreement between the theoretical and experimental breakthrough data; therefore, we do not report release rate coefficients in this work.

## 4. Results

### 4.1. Colloid and porous medium characterization

The size and zeta potential of the silica-coated zirconia colloids in the influent and effluent reservoirs and selected samples were consistent during the experiment. Consistent size indicates that the silica-coated colloids did not aggregate during the experiment, neither in the influent reservoir nor in the porous medium. Consistent zeta

potential indicates that the silica coatings did not deteriorate during the experiment. Deterioration of the silica coating would have led to a reduction in zeta potential as the underlying zirconia ($pH_{pzc} = 6.7$; Parks, 1965) contributed to surface charge and, ultimately, to aggregation.

Specific conductance of the influent and effluent reservoirs and selected samples was consistent during the experiment, indicating no significant ion exchange, precipitation, or dissolution reactions. Solution pH was constant in the influent reservoir (pH 6.2), but ranged from 5.7 to 6.2 in the effluent reservoir and samples. Total iron concentration in the effluent remained below or near the detection limit of 1.0 μg $l^{-1}$, indicating that the ferric oxyhydroxide coating on the porous media was stable during the experiment.

Measurements of the ferric oxyhydroxide surface coating fraction were similar to the estimates based on the mixing proportions and surface coverage of the coated grains (Table 1). The surface coating fractions are based on counts of a minimum of 4000 grains for each layer. Both before and after mixing of the coated and uncoated grains, the average surface coating of an individual coated grain was 75 ± 5%. For the upper layer, only nine coated grains at about 75% surface coating each were detected among 4820 grains counted. The reducible Fe(III) content of the mixed sands followed the trend of the ferric oxyhydroxide surface coating fraction, with the exception of the upper layer (Table 1). The mixed sand of upper layer contained slightly less reducible Fe(III) than the uncoated sand, but the difference was not significant. X-ray diffraction analysis detected only goethite (α-FeOOH) on the coated grains, but other amorphous ferric oxyhydroxides may have been present.

### 4.2. Tracer breakthrough data

Tritiated water travel times were similar in the three layers (Fig. 3). Only those data points necessary to define the tracer breakthrough curves are shown; more data for $C\,C_0^{-1}$ near zero or one are not shown. Over the first 5 cm of transport in each layer, the velocity of the tritium tracer was slightly accelerated relative to the transport over the 45–125-cm transport distances, perhaps because of improper mixing in the influent reservoir. The mean value of the longitudinal dispersivity $\alpha_L$ determined from nine breakthrough curves was $8.5 \pm 0.3 \times 10^{-4}$ m, where the error is the standard error of the fitted value. Because tritiated water breakthrough was similar in the three layers, this estimate of $\alpha_L$ was used throughout the tank for determination of the colloid deposition parameters.

### 4.3. Colloid breakthrough data

The experimental colloid breakthrough curves (Fig. 3) show the features expected for colloid transport controlled initially by clean-bed filtration and later by blocking. The details of a single colloid breakthrough curve (middle layer, 45 cm transport distance) are shown in Fig. 4 for clearer description. Prior to tracer breakthrough, the measured colloid concentration is near the background $C\,C_0^{-1}$ for zirconium. Because the background zirconium concentration is relatively high, the "initial breakthrough" of the colloids coincident with the tracer is not observed. The model shows this initial breakthrough beginning at $C\,C_0^{-1} = 10^{-9}$. At about 16 days, the measured colloid concentration begins a rapid increase to a plateau (the "blocking breakthrough") at about $C\,C_0^{-1} = 0.6–0.7$. The

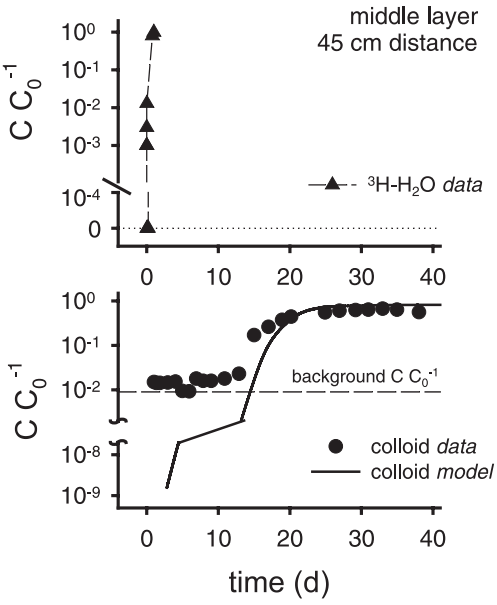


Fig. 4. Tritium tracer and silica-coated zirconia colloid breakthrough at the 45-cm transport distance in the middle layer of the aquifer tank. The tracer breakthrough data are presented on a combined linear and logarithmic $C\,C_0^{-1}$ axis to show the concentration below detection limit in the first sample. The colloid breakthrough data are shown with the colloid detection limit in terms of $C\,C_0^{-1}$.

rapid increase represents the onset of blocking effects—an increasing number of colloids are avoiding deposition as attachment sites are rapidly filled. In these experiments, the time to the blocking breakthrough increased as the favorable surface area fraction of the layers increased (Fig. 3). Finally, at the plateau for which $C\,C_0^{-1}$ appears constant, colloid concentration is actually increasing very slowly toward complete breakthrough ($C\,C_0^{-1} = 1$) as the final available deposition sites over the first 45 cm are slowly filled. Usually, this final trend is not demonstrated well by the data, but it is shown by the model-predicted breakthrough curves (more apparent in Fig. 3). The plateau in colloid concentration decreased with distance.

Colloid concentrations measured in sampling ports near the interfaces between layers (5 cm above and below the interface) showed concentrations similar to those measured in the center of each layer, indicating that transverse dispersion was not significant over the 1.65 m transport distance.

### 4.4. Colloid breakthrough modeling

Fig. 3 shows the theoretical colloid breakthrough curves generated by the colloid transport model employing the deposition parameters ($k_f$, $k_u$, $\lambda_{upper}$, $\lambda_{middle}$, and $\lambda_{lower}$; Table 1, Table 3) estimated with $k_f$ calculated by colloid filtration theory. Theoretical colloid breakthrough curves generated with the parameters optimized by the complete inverse solution were essentially indistinguishable from those shown in Fig. 3. The

reasonably good agreement between the model-predicted and experimental breakthrough curves suggest that the one-dimensional model was adequate in emulating the colloid transport behavior in the aquifer tank. In addition, the one-dimensional model is adequate because no transverse dispersion of colloids and tracer was measured for the sample port spacings used in the aquifer tank.

The time to the blocking breakthrough was adequately portrayed by the model at many, but not all, of the sampling locations (Fig. 3). At the 5-cm transport distance, the model predicted colloid breakthrough that was substantially faster than the observed breakthroughs in all three layers. At the 45-, 85-, and 125-cm transport distances (the distances at which the model parameters were fit), the model predicted the time to blocking breakthrough fairly well with the single values of $k_f$ and $k_u$, and the mean value of $\lambda$ for each layer, although with insufficient data, was collected at some sampling locations to fully verify the model predictions. At the 165-cm transport distance, the time to blocking breakthrough was predicted fairly well for all layers. In the middle layer, where the favorable surface area fraction was greatest, the model correctly predicted that colloid concentrations up to 95 days were close to zero.

The model predicts a decline in the colloid concentration of the plateau with distance in each layer. This trend is confirmed by some of the data, although some contradictions occurred, and in some cases, the data was not sufficiently complete to verify the model predictions. At the 5-cm distance, the model slightly overestimates the colloid concentration at the plateau in all layers. In the upper layer, the decrease in the colloid concentration plateau is overestimated by the model at the longer distances. In the middle layer, the model does not match the data particularly well for the 45- and 85-cm distances because the plateau at 45 cm occurs at a colloid concentration less than that occurring at 85 cm.

### 4.5. Colloid transport parameter identification

The two inverse solution techniques provided similar estimates of $\lambda$, the fraction of surface area favorable for colloid deposition for the middle and the lower layers (Table 1). The errors reported for $\lambda$ are the standard deviations of the three values determined for the 45-, 85-, and 125-cm transport distances for each layer. The estimated $\lambda$ values are also in

Table 3
Identification of attachment rate coefficients, single collector efficiencies, and collision efficiencies for favorable and unfavorable surface areas by two methods

| Parameter estimation procedure | Favorable surface area | | | Unfavorable surface area | | |
|---|---|---|---|---|---|---|
| | $k_f$ (m day$^{-1}$) | $\eta_f$ | $\alpha_f$ | $k_u$ (m day$^{-1}$) | $\eta_u$ | $\alpha_u$ |
| $k_f$ determined by complete inverse solution | $\mathbf{0.11 \pm 0.04}$ | 0.83 | 3.4 | $\mathbf{3.2 \pm 0.5 \times 10^{-5}}$ | $2.4 \times 10^{-4}$ | $9.8 \times 10^{-4}$ |
| $k_f$ determined by colloid filtration theory | *0.033* | *0.246* | *1* | $\mathbf{3.4 \pm 0.8 \times 10^{-5}}$ | $2.7 \times 10^{-4}$ | $1.1 \times 10^{-3}$ |

Entries in bold represent the model-fit values. Entries in italics represent the values assumed for and calculated by colloid filtration theory. Conversions between $k_i$ and $\eta_i$, where $i$ represents favorable ($f$) or unfavorable ($u$) surface area, were made with Eq. (4). Calculations of collision efficiencies ($\alpha_f$, $\alpha_u$) were made for a single collector efficiency $\eta_0 = 0.246$ calculated with Eq. (5).

close agreement with the experimentally determined values of $\lambda$ for the middle and lower layers. Agreement between the inverse solution techniques and the experimentally determined value of $\lambda_{upper}$ was not particularly good.

The two inverse solution provided similar estimates of $k_u$, the unfavorable deposition rate coefficient (Table 3). The value of $k_f$ estimated by the complete inverse solution did not agree well with the value of $k_f$ calculated by colloid filtration theory, but identification of $\lambda$ and $k_u$ was relatively insensitive to $k_f$. Errors reported for $k_f$ (fit by the complete inverse solution) and $k_u$ (fit by both inverse solutions) are the standard deviations of the nine values determined for the three layers at the 45-, 85-, and 125-cm transport distances. There is a very little deviation in the values of $k_f$ and $k_u$ estimated at the various sampling ports.

## 5. Discussion

### 5.1. Dispersion

The longitudinal dispersivity determined for tritium was used to portray dispersion of the colloids. The suitability of solute dispersivities for colloids has been experimentally established (Morley et al., 1996) and accepted in the formulation of colloid and biocolloid transport models (Hornberger et al., 1992; Rehmann et al., 1999). This assumption should be valid only if the velocity of the groundwater flow is sufficient for mechanical dispersion, and not diffusion, to be the dominant contributor to the overall dispersion of the tritium and colloids.

The similarity between colloid concentrations measured in the center of each layer and those measured near the layer interfaces indicated that transverse dispersion of colloids was negligible over the length scale of the experiment. To reflect the negligible effect of transverse dispersion, the ratio of longitudinal to transverse dispersitivity was set at $\alpha_L/\alpha_T = 10$ in the two-dimensional model. This ratio is in the range (6–20) commonly reported in previous studies (Gelhar et al., 1992). The model was found to be quite insensitive to transverse dispersion as long as $\alpha_L/\alpha_T \geq 10$. The value of this tank experiment, with the three-layer heterogeneity as the two-dimensional feature, was diminished by the lack of observance of transverse dispersion by the sampling array (with sampling ports 5 cm away from adjacent layers). Sampling ports should have been placed closer to the interfaces to monitor for the relatively small amount of transverse dispersion that would have occurred over the 165-cm transport distance. However, there is a two-dimensional value in the confirmation that transverse dispersion would be negligible ($\alpha_L/\alpha_T \geq 10$) for transport distances of up to 165 cm.

### 5.2. Effect of geochemical heterogeneity on colloid transport

This experiment shows that the transport of colloids in porous media is strongly influenced by geochemical heterogeneity in the form of ferric oxyhydroxide coatings favorable to colloid deposition. As the favorable surface area fraction $\lambda$ increases from measured values of 0.14–8.3%, the time to the blocking breakthrough increases. In

assessing the role of geochemical heterogeneity in colloid transport, it is important to realize that most of the colloid attachment occurs on the favorable surface area. Because the ratio of $k_f/k_u$ (or $\alpha_f/\alpha_u$) is on the order of $10^3$ for a typical ferric oxyhydroxide-coated quartz system (Table 3), colloid deposition is dominated by the favorable surface area if $\lambda$ is greater than $10^{-3}$ (0.1%). Thus, small changes in the amount of favorable surface area can dramatically affect the time and colloid concentration for complete breakthrough (Mills et al., 1994; Johnson et al., 1996; Ryan et al., 1999; Elimelech et al., 2000). In these simulations and those of Sun et al. (2001a,b), colloid transport is most sensitive to variation of the favorable surface area fraction.

The blocking breakthrough occurs when the available surface area for deposition is rapidly decreasing (Ko et al., 2000). A rapid increase in the colloid surface concentration $\theta$ is closely followed by a rapid increase in the colloid concentration (the blocking breakthrough). When colloid deposition is dominated by favorable surface area, the time to blocking breakthrough should be related to the favorable surface area fraction. Compare the transport to 85 cm in middle and lower layers—an approximate doubling of the favorable surface area fraction from $\lambda_{meas} = 4.2 - 8.3\%$ resulted in an approximate doubling of the time to blocking breakthrough from 28 to 65 days (Fig. 3; blocking breakthrough defined as colloid concentration at 90% of the plateau in $C\ C_0^{-1}$).

The model clearly predicts that colloid concentration at the plateau following the blocking breakthrough steadily decreases with distance in each layer. This decrease represents the loss of mobile colloids, or the attenuation (irreversible deposition) of colloids, over distance. The data collected during this experiment generally support this model prediction, but some inconsistencies and missing data preclude definitive confirmation. The data collected in the lower layer provide the best confirmation of the model-predicted decrease in the plateau with distance. In the upper layer, data following the blocking breakthrough are sparse, but for the data collected, the colloid concentration of the plateaus decreases with distance. In the middle layer, the plateau at 45 cm is lower than the plateau at 85 cm. At 125 and 165 cm, the postblocking breakthrough plateau was never reached.

### 5.3. Parameter identification: favorable surface area fraction

The model-fits for the favorable surface area fraction compare well with the values measured by electron microprobe for middle and lower layers, but not for the upper layer. For the upper layer, the model-fit values are substantially larger than the measured value ($\lambda_{upper} = 1.2 \pm 0.8\%$ or 1.8% versus $\lambda_{meas} = 0.14\%$), even when the large error on $\lambda_{upper}$ is considered (Table 1).

The discrepancy between the measured and model-fit values of the favorable surface area fraction indicates that the uncoated sand contains favorable attachment surface area that was not detected by the electron microprobe analysis. Recall that the electron microprobe analysis detected no bright iron-rich coatings on any of the uncoated sand grains. The Fe(III) extraction procedure did remove 3.6 mmol $kg^{-1}$ of Fe(III), an amount comparable to the amount of ferric iron removed from Cape Cod glacial outwash sands (Coston et al., 1995; Pieper et al., 1997), but the uncoated sand has none of the reddish-orange tinge of the Cape Cod sand (it is possible that the extraction removed some structural Fe(III) from the mica mineral grains).

Instead, we suspect that the uncoated sand contained favorable attachment surface area in the form of mica (muscovite and biotite) edges. Phyllosilicates, like muscovite and biotite, possess faces characterized by ''permanent'' negative charge arising from isomorphic substitution and edges characterized by amphoteric silica and alumina surface functional groups. The edges of mica minerals are positively charged below neutral pH (e.g., Anderson and Sposito, 1992; Ilton and Veblen, 1994), presumably as a result of protonation of the alumina surface hydroxyls. If edges comprise 10% of the muscovite and biotite surface area, then the 8% mica fraction (by number for grains of roughly equal size) could contribute a 0.8% favorable surface area fraction.

In the upper layer sand mixture, the favorable surface area attributed to mica edges would be much greater than the $\lambda_{meas} = 0.14\%$ attributed to ferric oxyhydroxide coatings by electron microprobe analysis resulting in favorable surface area fractions much closer to the model-fit $\lambda_{upper}$ value determined by complete inverse solution, but still considerably smaller than the $\lambda_{upper}$ value determined by initiating the inverse solution with a calculated $k_f$ value. Adding the same amount of favorable surface area attributed to mica edges to the sand mixtures in the middle and lower layers still allows good agreement between the measured and model-fit values of the favorable surface area fraction for those layers.

### *5.4. Parameter identification: deposition rate coefficients*

The $k_f$ value determined by the complete inverse solution corresponds to a collision efficiency of $\alpha_f = 3.4$, whereas $\alpha_f = 1$ is assumed for the inverse solution initiated by calculation of $k_f$ (Table 3). Collision efficiencies greater than one occur under favorable deposition conditions (Elimelech, 1991; Ko and Chen, 2000); however, collision efficiencies as high as 3.4 have not been measured, even at very low ionic strength where attractive electrostatic interactions promote collision efficiencies greater than one. The high values of $k_f$ and $\alpha_f$ predicted by the complete inverse solution are probably the result of nonuniformity of the aquifer grains. For the calculation of $\eta_0$, filtration theory assumes spherical grains of uniform size. Nonsphericity of grains results in greater grain surface area, and hence, greater colloid deposition. Nonuniform grain size distributions, particularly those skewed toward smaller grain sizes, also result in greater surface area and deposition.

The values of $k_u$ estimated by the two inverse solutions are nearly the same despite the difference in $k_f$ values determined by the inverse solution or calculated for the inverse solution. The $\alpha_u$ values corresponding to these $k_u$ values are quite similar to collision efficiencies measured for silica colloids in pure quartz sand at millimolar ionic strength and slightly acidic to near-neutral pH (Saiers et al., 1994a; Johnson et al., 1996; Elimelech et al., 2000).

## 6. Summary

The transport of colloids at distances up to 165 cm in a geochemically heterogeneous porous medium, consisting of three layers of sand coated to different extents by ferric oxyhydroxide, depended strongly on the fraction of coated surface area. The colloid and

tritium tracer transport parameters were estimated with acceptably low uncertainty by a series of one-dimensional inverse analyses of well-defined tracer and colloid breakthroughs. In contrast, a simultaneous two-dimensional inverse analysis of all breakthrough data produced transport parameter estimates with unacceptably high uncertainties. One-dimensional inverse analyses successfully predicted the favorable surface area fraction for the two layers with favorable surface area fractions of 4.2% and 8.3%. For the layer with a favorable surface fraction of only 0.14%, the model predicted much higher favorable surface area fractions ($1.2 \pm 0.8\%$ by complete inverse analyses and $1.7 \pm 0.7\%$ by inverse analyses initiated by calculation of the deposition rate coefficient for the favorable surface area). This discrepancy may be caused by the presence of mica in the sand—the mica edges may act as favorable deposition sites. The favorable deposition rate coefficient estimated by the model may be overestimated owing to nonsphericity and nonuniform size of the porous media grains. Both of these deviations from the assumptions of colloid filtration theory increase grain surface area and hence deposition. The unfavorable deposition rate coefficient estimated by the model agrees well with deposition rate coefficients for deposition of silica colloids on quartz sand under similar chemical conditions. Overall, the model captured the essential features of the colloid breakthroughs in this layered geochemically heterogeneous porous medium.

## Acknowledgements

This research was supported by the grants from the National Science Foundation (EAR-9418472) and the US Environmental Protection Agency (CR824593-01). We thank Ning Sun (Yale University) for preliminary model runs to assist experimental planning, Robin Magelky for the development of the silica-coated zirconia colloids, John Drexler and Paul Boni (University of Colorado) for electron microprobe and X-ray diffraction assistance, the University of Colorado Summer Minority Access to Research Training Program for providing two undergraduate research assistants, and James Saiers (Yale University) and an anonymous reviewer for review comments that improved the manuscript.

## References

Abdel-Salam, A., Chrysikopoulos, C.V., 1995. Modeling of colloid and colloid-facilitated contaminant transport in a two-dimensional fracture with spatially variable aperture. Transp. Porous Media 20, 197–221.

Anderson, S.J., Sposito, G., 1992. Proton surface-charge density in soils with structural and pH-dependent charge. Soil Sci. Soc. Am. J. 56, 1437–1443.

Bales, R.C., Hinkle, S.R., Kroeger, T.W., Stocking, K., Gerba, C.P., 1991. Bacteriophage adsorption during transport through porous media: chemical perturbations and reversibility. Environ. Sci. Technol. 25, 2088–2095.

Bhattacharjee, S., Kim, A.S., Elimelech, M., 1999. Concentration polarization of interacting solute particles in cross-flow membrane filtration. J. Colloid Interface Sci. 212, 81–99.

Corapcioglu, M.Y., Jiang, S., 1993. Colloid-facilitated groundwater contaminant transport. Water Resour. Res. 29, 2215–2226.

Coston, J.A., Fuller, C.C., Davis, J.A., 1995. $Pb^{2+}$ and $Zn^{2+}$ adsorption by a natural aluminum- and iron-bearing surface coating on an aquifer sand. Geochim. Cosmochim. Acta 59, 3535–3547.

Elimelech, M., 1991. Kinetics of capture of colloidal particles in packed beds under attractive double layer interactions. J. Colloid Interface Sci. 146, 337–351.

Elimelech, M., Gregory, J., Jia, X., Williams, R., 1995. Particle Deposition & Aggregation. Measurement, Modelling and Simulation. Butterworth-Heinemann, Oxford, England.

Elimelech, M., Nagai, M., Ko, C.-H., Ryan, J.N., 2000. Relative insignificance of mineral grain zeta potential to colloid transport in geochemically heterogeneous porous media. Environ. Sci. Technol. 34, 2143–2148.

Garabedian, S.F., LeBlanc, D.R., Gelhar, L.W., Celia, M.A., 1991. Large-scale natural gradient tracer test in sand and gravel, Cape Cod, Massachusetts: 2. Analysis of spatial moments for a nonreactive tracer. Water Resour. Res. 27, 911–924.

Gelhar, L.W., Welty, C., Rehfeldt, K.R., 1992. A critical review of data on field-scale dispersion in aquifers. Water Resour. Res. 28, 1955–1974.

Grindrod, P., 1993. The impact of colloids on the migration and dispersal of radionuclides within fractured rock. J. Contam. Hydrol. 13, 167–181.

Harvey, R.W., Garabedian, S.P., 1991. Use of colloid filtration theory in modeling movement of bacteria through a contaminated sandy aquifer. Environ. Sci. Technol. 25, 178–185.

Higgo, J.W.W., Williams, G.M., Harrison, I., Warwick, P., Gardiner, M.P., 1993. Colloid transport in a glacial sand aquifer. Laboratory and field studies. Colloids Surf., A Physicochem. Eng. Asp. 73, 179–200.

Hornberger, G.M., Mills, A.L., Herman, J.S., 1992. Bacterial transport in porous media: evaluation of a model using laboratory observations. Water Resour. Res. 28, 915–938.

Ilton, E.S., Veblen, D.R., 1994. Chromium sorption by phlogopite and biotite in acidic solutions at 25 °C: insights from X-ray photoelectron spectroscopy and electron microscopy. Geochim. Cosmochim. Acta 58, 2777–2788.

Johnson, P.R., Elimelech, M., 1995. Dynamics of colloid deposition in porous media: blocking based on random sequential adsorption. Environ. Sci. Technol. 11, 801–812.

Johnson, P.R., Sun, N., Elimelech, M., 1996. Colloid transport in geochemically heterogeneous porous media: modeling and measurements. Environ. Sci. Technol. 30, 3284–3293.

Ko, C.-H., Chen, J.Y., 2000. Dynamics of silica colloid deposition and release in packed beds of aminosilane-modified glass beads. Langmuir 16, 6906–6912.

Ko, C.-H., Bhattacharjee, S., Elimelech, M., 2000. Coupled influence of colloidal and hydrodynamic interactions on the RSA dynamic blocking function for particle deposition onto packed spherical collectors. J. Colloid Interface Sci. 229, 554–567.

Loveland, J.P., Ryan, J.N., Amy, G.L., Harvey, R.W., 1996. The reversibility of virus attachment to mineral surfaces. Colloids Surf., A Physicochem. Eng. Asp. 107, 205–221.

Mills, W.B., Liu, S., Fong, F.K., 1991. Literature review and model (COMET) for colloid-metals transport in porous media. Ground Water 29, 199–208.

Mills, A.L., Herman, J.S., Hornberger, G.M., DeJesús, T.H., 1994. Effect of solution ionic strength and iron coatings on minerals grains on the sorption of bacterial cells to quartz sand. Appl. Environ. Microbiol. 60, 3300–3306.

More, J., Garbow, B., Hillstrom, K., 1980. User guide for MINPACK-1. Report ANL-80-74, Argonne National Laboratories Reports, Argonne, IL.

Morley, L.M., Hornberger, G.M., Mills, A.L., Herman, J.S., 1996. Effects of transverse mixing on transport of bacteria through heterogeneous porous media. Water Resour. Res. 34, 1901–1908.

Parks, G.A., 1965. The isoelectric points of solid oxides, solid hydroxides, and aqueous hydroxo complex systems. Chem. Rev. 65, 177–198.

Petzold, L.R., 1982. A description of DASSL: a differential/algebraic system solver. Report SAND82-8637, Sandia National Laboratories, Albuquerque, NM.

Pieper, A.P., Ryan, J.N., Harvey, R.W., Amy, G.L., Illangasekare, T.H., Metge, D.W., 1997. Transport and recovery of bacteriophage PRD1 in a sand and gravel aquifer: effect of sewage-derived organic matter. Environ. Sci. Technol. 31, 1163–1170.

Privman, V., Frisch, H.L., Ryde, N., Matijević, E., 1991. Particle adhesion in model systems: 13. Theory of multilayer deposition. J. Chem. Soc., Faraday Trans. 87, 1371–1375.

Rehmann, L.L.C., Welty, C., Harvey, R.W., 1999. Stochastic analysis of virus transport in aquifers. Water Resour. Res. 35, 1987–2006.

Ren, J., Packman, A.I., Welty, C., 2000. Correlation of colloid collision efficiency with hydraulic conductivity of silica sands. Water Resour. Res. 36, 2493–2500.

Ryan, J.N., Elimelech, M., 1996. Colloid mobilization and transport in groundwater. Colloids Surf., A Physicochem. Eng. Asp. 107, 1–52.

Ryan, J.N., Gschwend, P.M., 1991. Extraction of iron oxides from sediments using reductive dissolution by titanium(III). Clays Clay Miner. 39, 509–518.

Ryan, J.N., Elimelech, M., Ard, R.A., Harvey, R.W., Johnson, P.R., 1999. Bacteriophage PRD1 and silica colloid transport and recovery in an iron oxide-coated sand aquifer. Environ. Sci. Technol. 33, 63–73.

Ryan, J.N., Elimelech, M., Baeseman, J.L., Magelky, R.D., 2000. Silica-coated titania and zirconia colloids for subsurface transport field experiments. Environ. Sci. Technol. 34, 2000–2005.

Saiers, J.E., Hornberger, G.M., Liang, L., 1994a. First- and second-order kinetics approaches for modeling the transport of colloidal particles in porous media. Water Resour. Res. 30, 2499–2506.

Saiers, J.E., Hornberger, G.M., Harvey, C., 1994b. Colloidal silica transport through structured, heterogeneous porous media. J. Hydrol. 163, 271–288.

Schijven, J.F., Hassanizadeh, S.M., 2000. Removal of viruses by soil passage: overview of modeling, processes, and parameters. Crit. Rev. Environ. Sci. Technol. 30, 49–127.

Schijven, J.F., Medema, G.J., Vogelaar, A.J., Hassanizadeh, S.M., 2000. Removal of microorganisms by deep well injection. J. Contam. Hydrol. 44, 301–327.

Song, L., Elimelech, M., 1993. Dynamics of colloid deposition in porous media: modeling the role of retained particles. Colloids Surf., A Physicochem. Eng. Asp. 73, 49–63.

Song, L., Elimelech, M., 1994. Transient deposition of colloidal particles in heterogeneous porous media. J. Colloid Interface Sci. 167, 301–313.

Sun, N., Elimelech, M., Sun, N.-Z., Ryan, J.N., 2001a. A two-dimensional model of colloid transport in physically and geochemically heterogeneous porous media. J. Contam. Hydrol. 49, 173–199.

Sun, N., Sun, N.-Z., Elimelech, M., Ryan, J.N., 2001b. Sensitivity analysis and parameter identifiability for colloid transport in geochemically heterogeneous porous media. Water Resour. Res. 37, 209–222.

Yao, K.-M., Habibian, M.T., O'Melia, C.R., 1971. Water and wastewater treatment filtration: concepts and applications. Environ. Sci. Technol. 5, 1105–1112.

Yates, M.V., Yates, S.R., Wagner, J., Gerba, C.P., 1987. Modeling virus survival and transport in the subsurface. J. Contam. Hydrol. 1, 329–345.

Zhang, H., Schwartz, F.W., Wood, W.W., Garabedian, S.P., LeBlanc, D.R., 1998. Simulation of variable-density flow and transport of reactive and nonreactive solutes during a tracer test at Cape Cod, Massachusetts. Water Resour. Res. 34, 76–82.

Zwillinger, D., 1989. Handbook of Differential Equations. Academic Press, Chestnut, MA.